Time Reversal of Light with Linear Optics and Modulators

Mehmet Fatih Yanik and Shanhui Fan
Ginzton Laboratory, Stanford University, Stanford, California 94305, USA
(Received 18 May 2004; published 22 October 2004)

We introduce a new physical process that can perform a complete time-reversal operation on any electromagnetic pulse. The process uses only small refractive index modulations of linear optical elements. No nonlinear multiphoton effects such as four-wave mixing are required. The introduced process can be implemented on chip with standard semiconductor materials. Furthermore, the same process can be used to compress or expand the spectrum of electromagnetic waves while completely preserving the coherent information. We exhibit the time-reversal process by first-principles simulations of microcavity complexes in photonic crystals.

DOI: 10.1103/PhysRevLett.93.173903 PACS numbers: 42.70.Qs, 42.60.Da, 42.65.Hw

The capability to reverse a wave in time has profound scientific and technological implications. Examples of applications include detection through random media, adaptive optics, subwavelength focusing, and dispersion compensation [1–8]. In acoustics or electronics, where the frequencies are low, time reversal can be accomplished by electronic sampling, recording, and playing back [1,2]. For optical waves, on the other hand, since fields oscillate at higher frequencies, all the mechanisms for time reversal up to now required nonlinear processes such as near-degenerate four-wave mixing [9]. Such nonlinear processes can phase conjugate a monochromatic wave. However, for a pulse, phase matching needs to be satisfied over the entire pulse bandwidth, which presents a challenge to the development of nonlinear materials. In addition, such processes require high-power lasers, which limit on-chip integration.

Recently, it was discovered that the spectrum of a photon can be modified when the index of a photonic crystal is modulated [10–12]. In particular, we have shown that such a dynamic photonic system, when appropriately designed, can stop and release light pulses while completely preserving coherent information in the optical domain [12]. Here, we show that a similar system can be used to time reverse optical pulses by only linear optics and electro-optic modulators. No knowledge of the time-dependent phase or amplitude of the light is necessary. Thus electronic or optical sampling at optical frequencies is not required. Moreover, no nonlinear multiphoton process is required here, which greatly broadens the choices of materials. A fundamental roadblock in developing integrated photonics has been that each information processing task requires a distinct material system. Integration of multiple tasks on a single chip therefore becomes extremely difficult. Here, we show that dynamic photonic crystals, which can be constructed in any material system where index can be tuned slightly ($\delta n/n < 10^{-4}$), can perform sophisticated tasks such as time reversal and pulse stopping, and may eventually provide a platform for on-chip optical information processing.

Consider a pulse $\psi(t) = A(t, x)e^{i(\omega_c t - k_c x)} + \text{c.c.}$, where $e^{i(\omega_c t - k_c x)}$ is the carrier wave with frequency ω_c and wave vector k_c, and $A(t, x)$ is the complex envelope that carries information. The envelope $A(t, x)$ can be decomposed into its Fourier components as

$$A(t, x) = \sum_k A_k e^{-i(k-k_c)x} e^{i\Delta\omega_k t}. \quad (1)$$

Here k is a wave vector component, and $\Delta\omega(k) = \omega(k) - \omega_c$ is the frequency detuning. The time-reversed pulse envelope $A(-t)$ has a Fourier decomposition of

$$A(-t, x) = \sum_k A_k e^{-i(k-k_c)x} e^{-i\Delta\omega_k t}. \quad (2)$$

Thus time reversal can be achieved if the frequency of a Fourier component with detuning $\Delta\omega_k$ is converted to a new frequency with detuning $-\Delta\omega_k$ and if such frequency conversion is performed for all Fourier components of the pulse [9]. In order to preserve wave vector information, such a conversion process should be translationally invariant. Therefore, the pulse should be inside the system during the time-reversal process.

In order to achieve such frequency conversion, we consider a system consisting of two translationally invariant subsystems A and B (Fig. 1). Each subsystem is a coupled resonator optical waveguide (CROW) structure [13,14], with nearest-neighbor evanescent coupling rates of α_A and α_B, respectively. The subsystems also evanescently couple to each other with a coupling rate of β. The dynamics of the field amplitudes a_i and b_i for cavities A and B in the ith unit cell can be expressed using coupled mode theory:

$$\frac{da_i}{dt} = i\omega_A a_i + i\alpha_A(a_{i-1} + a_{i+1}) + i\beta b_i - \gamma_A a_i, \quad (3)$$

$$\frac{db_i}{dt} = i\omega_B b_i + i\alpha_B(b_{i-1} + b_{i+1}) + i\beta a_i - \gamma_B b_i. \quad (4)$$

 0031-9007/04/93(17)/173903(4)$22.50

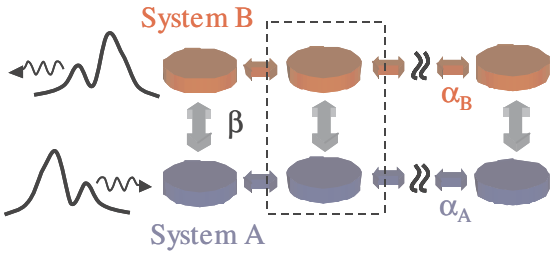

FIG. 1 (color). Schematic of a tunable microcavity system used to time reverse light. The disks represent cavities, and the arrows indicate available evanescent coupling between the cavities. The system consists of two subsystems A and B represented by blue and red colors. The dashed box indicates a unit cell.

Here ω_A and ω_B are the resonance frequencies, and γ_A and γ_B are the loss rates for the cavities A and B, respectively. For time reversal, we choose $\alpha_A = -\alpha_B \equiv -\alpha$ such that the two CROW waveguides have opposite dispersion relations. The eigenfrequencies $\omega_{\pm,k}$ of the system with a wave vector k can be derived as

$$\omega_{\pm,k} = \frac{1}{2}[\omega_{A,k} + \omega_{B,k} + i(\gamma_A + \gamma_B) \pm \sqrt{[\omega_{A,k} - \omega_{B,k} + i(\gamma_A - \gamma_B)]^2 + 4\beta^2}], \quad (5)$$

where $\omega_{A,k} = \omega_A - 2\alpha\cos(k\ell)$ and $\omega_{B,k} = \omega_B + 2\alpha\cos(k\ell)$ are the frequency bands of the subsystems A and B by themselves, respectively. ℓ is the distance between the nearest-neighbor cavities in subsystem A or subsystem B. The shapes of the bands become independent of losses when γ_A and γ_B are equal, which can be adjusted externally.

In this system, a pulse can be time reversed by the following process: We start with $\omega_A - \omega_B \ll -|\beta|$, such that the lower band exhibits the characteristic of the subsystem A [Fig. 2(a)]. By placing ω_A at the pulse carrier frequency ω_c [Fig. 2(a)], the lower band can accommodate the pulse, with each spectral component of the pulse occupying a unique wave vector. After the pulse is in the system, we vary ω_A and ω_B until $\omega_A - \omega_B \gg |\beta|$ [Fig. 2(c)], at a rate that is slow compared with the frequency separation between the lower and the upper bands. [The frequency separation reaches minimum $2|\beta|$ when $\omega_A = \omega_B$, Fig. 2(b)]. The modulation of the cavity resonances preserves translational symmetry. Therefore, cross talk between different wave vector components of the pulse is prevented. Also, the slow modulation rate ensures that each wave vector component of the pulse follows only the lower band, with negligible scattering into the upper band (i.e., the system evolves in an adiabatic [15] fashion). Consequently, an initial state with a wave vector k and detuning $\Delta\omega_k$ evolves into a final state with the same wave vector but an opposite detuning of $-\Delta\omega_k$. The spectrum of the incident pulse is thus inverted while the information encoded in the pulse is preserved. Such a spectral inversion process generates a time-reversed version of the original pulse, which moves in subsystem B backward to its original propagation direction, and exits the system. The modulation can follow any adiabatic trajectory in time and can have a narrower spectrum than the pulse.

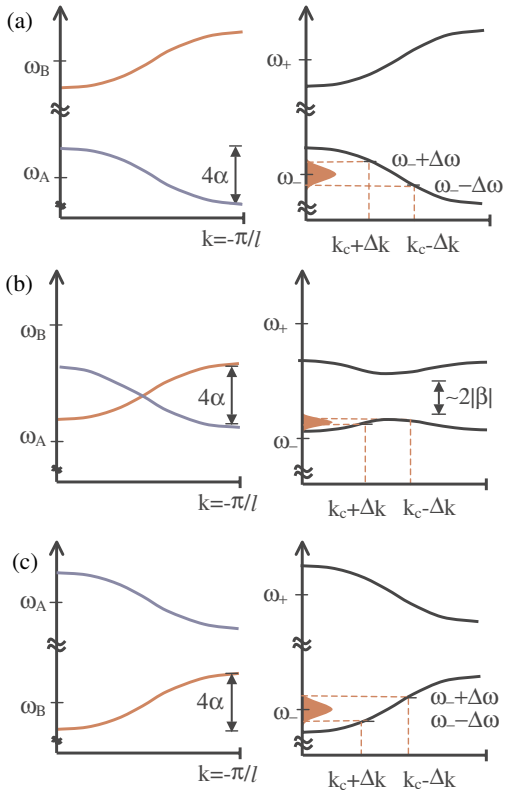

FIG. 2 (color). ω_A and ω_B are the resonance frequencies for individual cavities in subsystems A and B, respectively, and k is the wave vector. In the left panels, the red and blue curves correspond to the bands for subsystems A and B by themselves, respectively. The cavities in A are coupled to each other via a negative rate. The cavities in B are coupled to each other via a positive rate. The right panels are the band structures ω_+ and ω_- of the coupled system. The figure includes three cases: (a) $\omega_A - \omega_B \ll -|\beta|$, (b) $\omega_A \approx \omega_B$, and (c) $\omega_A - \omega_B \gg |\beta|$.

We implement such a system in a photonic crystal, as shown in Fig. 3. Increasing the radius of one of the high index rods to $0.5a$ generates a singly degenerate mode at $\omega_0 = 0.286(2\pi c/a)$. We construct two CROW waveguides, each consisting of an array of such cavities (Fig. 3). These two CROW waveguides form the subsystems A and B. Coupling between two neighboring cavities of the subsystem A occurs through a barrier of five rods ($\ell = 6a$), with a rate of $\alpha_A = -1.89 \times 10^{-3}(2\pi c/a)$. The two subsystems A and B are coupled

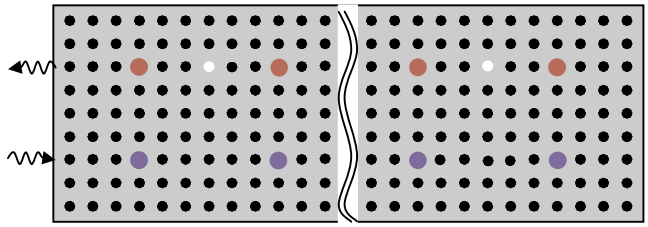

FIG. 3 (color). An implementation of the general system of Fig. 1 in a two-dimensional photonic crystal. The crystal consists of high index ($n = 3.4$) rods in a low index material ($n = 1.5$) indicated by the gray background. The black dots indicate the dielectric rods. These rods have a radius of $0.2a$, where a is the lattice constant. The blue and red dots represent dielectric rods with a radius of $0.5a$ and with a tunable index near 3.4. These dots form the subsystems A and B. The white holes indicate air cylinders with radius $0.2a$.

with a rate of $\beta = -1.89 \times 10^{-3}(2\pi c/a)$. The resonant frequencies of the cavities can be tuned by refractive index modulations of the dielectrics within the cavities. In subsystem B, we introduce air cylinders with radius $0.2a$ in the middle of the barriers. In a CROW waveguide, the band-edge state at $k = 0$ has significant energy in the center of the barriers, while the band-edge state at $k = \pi/\ell$ has a nodal plane at the same location. Thus, by adjusting the dielectric between the cavities, the dispersion of the CROW waveguide can be strongly affected. Our choice for the radius of the air cylinders yields $\alpha_B = 1.89 \times 10^{-3}(2\pi c/a) = -\alpha_A$.

We simulate a system with 100 pairs of cavities using finite-difference time-domain (FDTD) method [16], which solves Maxwell's equations without approximation. The subsystems are terminated by introducing a loss rate equal to $|\alpha_{A,B}|$ in the last cavities. This provides a perfect absorbing boundary condition. Initially, we generate an asymmetric pulse [Fig. 4(a)] by exciting the first cavity. (The process is independent of the pulse shape.) The excitation has a large peak at $t = 0.5t_{\text{pass}}$ and a smaller peak at $t = 0.75t_{\text{pass}}$, where t_{pass} is the traversal time of the pulse through the system without any index modulation. While the pulse is generated, the subsystem A is in resonance with the pulse frequency while the subsystem B is kept detuned. The field is concentrated in the subsystem A [Fig. 4(b), upper panel; $t = 0.8t_{\text{pass}}$], and the pulse propagates at a group velocity of $2\alpha_A\ell$. After the pulse is generated, we gradually tune the subsystem B into resonance with the pulse while detuning the subsystem A out of resonance [Fig. 4(a); $t = 1.25t_{\text{pass}}$]. At the end of this process, the field is transferred from the subsystem A to the subsystem B [Fig. 4(b), lower panel; $t = 1.2t_{\text{pass}}$]. We used a modulation $\exp[-t^2/t_{\text{mod}}^2]$, where $t_{\text{mod}} = 10/\beta$, which is sufficient to preserve adiabaticity. The pulse at the exit of the subsystem B shows the perfect time-reversed temporal shape of the initial pulse at the entrance of the subsystem A [Fig. 4(a)]. In the FDTD simulations, to

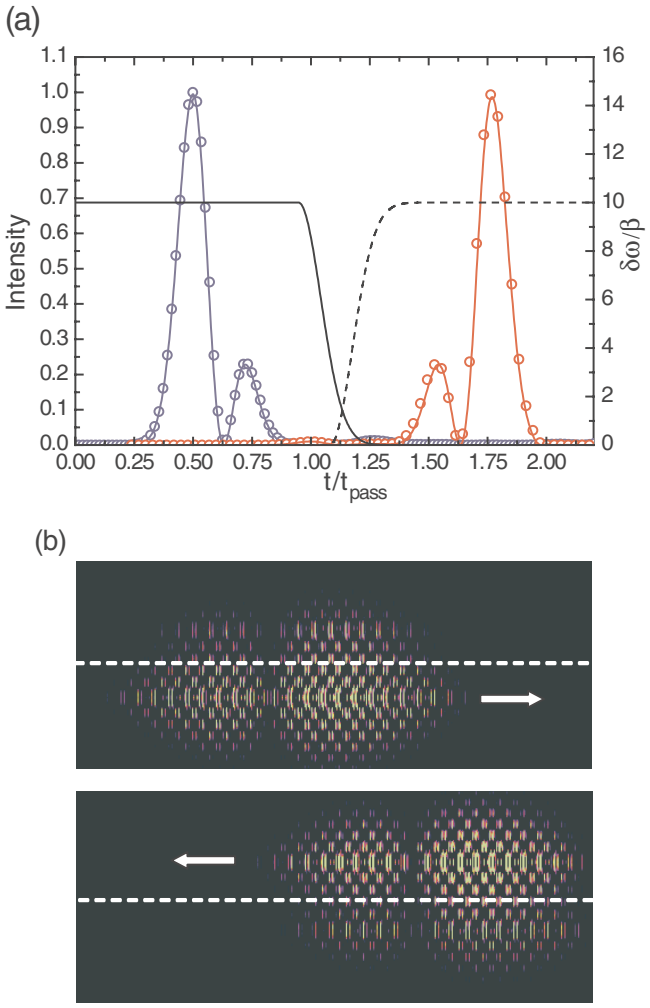

FIG. 4 (color). Propagation of an optical pulse through a coupled microcavity complex in a photonic crystal system as the resonance frequencies of the cavities are varied. The photonic crystal consists of 100 cavity pairs. (a) The dashed and solid black lines represent the variation of resonance frequencies $(\omega_{A,B} - \omega_c)/\beta \equiv \delta\omega/\beta$ as a function of time, respectively. The blue and the red lines represent the electromagnetic intensity as recorded in the middle of subsystems A and B, respectively. t_{pass} is the traversal time of the pulse through the system when no index modulation is applied. Open circles are FDTD results, and the red and blue lines are from coupled mode theory. (b) Snapshots of the electric field distributions in the photonic crystal at $t = 0.8t_{\text{pass}}$ and $t = 1.2t_{\text{pass}}$, in the upper and lower panels, respectively. The dimensions of the images along the propagation direction are compressed. Yellow represents large positive electric fields. The same color scale is used for both panels. The arrows indicate the propagation direction of the pulse, and the dashed lines represent the locations halfway in between subsystems A and B.

make the total simulation time feasible, we choose a large index modulation of about 6% and a modulation rise time of about 10 ps. We have also performed coupled mode theory calculations using Eqs. (1)–(4), where the effects of index change are taken into account by the modulation of the resonant frequencies, while the coupling constants are kept unchanged. This approach is valid as long as the frequency change is small. The results show excellent agreement with FDTD [Fig. 4(a)].

Coupled mode theory allows us to determine the system requirements in practical optoelectronic devices, since the modulation strengths $(\delta n/n)$ are typically less than 10^{-4} [17]. The number of cavities is determined by the pulse length and the duration of the time-reversal process. The duration of time reversal can be reduced by using a large β since the fastest modulation rate is limited by β. The largest coupling β that can be used is limited by the strength of index modulations. To accommodate a pulse, the coupling constants $|\alpha_{A,B}|$ need to be larger than the bandwidth of the pulse. In a photonic band gap, both $|\alpha_{A,B}|$ and β decrease exponentially with the distance between the cavities and also depend on the band gap size. The coupling constants can therefore be designed by choosing appropriate distances and lattice constants in photonic crystals [18]. With a refractive index modulation on the order of 10^{-4} at a maximum modulation speed of 100 GHz, about 100 microcavities is sufficient to time reverse an pulse with a 20 GHz bandwidth centered at 200 THz. Independent modulation of only two sets of cavities (i.e., A and B in Fig. 1) is required. With electro-optical modulation of high-Q microcavities [19], chip-scale implementation of such systems is foreseeable. In addition to time reversal, bandwidth compression or expansion can be achieved by choosing $|\alpha_B| \neq |\alpha_A|$. The use of dynamic photonic crystals thus allows new possibilities for spectral engineering of optical pulses. The underlying ideas and scheme here are applicable to all wave phenomena, including acoustics and microwave signals.

The simulations were performed at the Pittsburgh Supercomputing Center through the support of a NSF-NRAC grant.

[1] M. Fink, IEEE Trans. Ultrason. Ferroelectr. Freq. Control **39**, 555 (1992).
[2] I. Freund, J. Opt. Soc. Am. A **9**, 456 (1992).
[3] J. de Rosny and M. Fink, Phys. Rev. Lett. **89**, 124301 (2002).
[4] G. S. Agarwal, A. T. Friberg, and E. Wolf, J. Opt. Soc. Am. **73**, 529 (1983).
[5] A. Yariv, Appl. Phys. Lett. **28**, 88 (1976).
[6] R. A. Fisher, *Optical Phase Conjugation* (Academic, San Diego, 1984).
[7] B. Ya. Zel'dovich, N. F. Pilipetsky, and V. V. Shkunov, *Principles of Phase Conjugation* (Springer-Verlag, Berlin, 1985).
[8] D. M. Marom, IEEE J. Quantum Electron. **7**, 683 (2001).
[9] D. M. Pepper, *Laser Handbook* (North-Holland Physics, Amsterdam, 1988), Vol. 4, p. 333.
[10] E. J. Reed, M. Soljacic, and J. D. Joannopoulos, Phys. Rev. Lett. **90**, 203904 (2003).
[11] E. J. Reed, M. Soljacic, and J. D. Joannopoulos, Phys. Rev. Lett. **91**, 133901 (2003).
[12] M. F. Yanik and S. Fan, Phys. Rev. Lett. **92**, 083901 (2004).
[13] N. Stefanou and A. Modinos, Phys. Rev. B **57**, 12 127 (1998).
[14] A. Yariv, Y. Xu, R. K. Lee, and A. Scherer, Opt. Lett. **24**, 711 (1999).
[15] A. Messiah, *Quantum Mechanics* (Interscience, New York, 1963).
[16] A. Taflove and S. C. Hagness, *Computational Electrodynamics* (Artech House, Norwood, MA, 2000).
[17] S. L. Chuang, *Physics of Optoelectronic Devices* (Interscience, New York, 1995).
[18] J. D. Joannopoulos, R. D. Meade, and J. N. Winn, *Photonic Crystals: Molding the Flow of Light* (Princeton University Press, New Jersey, 1995).
[19] V. Ilchenko *et al.*, Proceedings of the 28th Annual GOMACTech Conference, Florida, 2003.